Exclusive J/Ψ and $\Psi(2s)$ photo-production as a probe of QCD low x evolution equations

Martin Hentschinski and Emilio Padrón Molina

Departamento de Actuaria, Física y Matemáticas, Universidad de las Americas Puebla, Santa Catarina Martir, 72820 Puebla, Mexico

(Received 10 November 2020; accepted 22 March 2021; published 13 April 2021)

We investigate photo-production of vector mesons J/Ψ and $\Psi(2s)$, based on both HERA and LHC data, using 2 fits of unintegrated gluon distributions. The latter are subject to nonlinear Balitsky-Kovchegov evolution (Kutak-Sapeta gluon; KS) and linear next-to-leading order Balitsky-Kuraev-Fadin-Lipatov evolution (Hentschinski-Sabio Vera-Salas; HSS gluon) respectively. Apart from extending previous studies to the case of radially excited charmonium $\Psi(2s)$, we further use an improved set of charmonium wave functions, provided in the literature, and give an estimate of the uncertainties associated with the energy dependence of the HSS gluon. While we observe that the difference between linear and non-linear evolution somehow diminishes and a clear distinction between both HSS and KS gluon is not possible using the currently available data set, we find that the differences between both gluon distributions are enhanced for the ratio of the photo-production cross sections of $\Psi(2s)$ and J/Ψ vector mesons.

DOI: 10.1103/PhysRevD.103.074008

I. INTRODUCTION

Due to its large center of mass energy, the Large Hadron Collider (LHC) provides a unique opportunity to explore the dynamics of strong interactions in the high energy or Regge limit. For a process with a hard scale, which renders the strong coupling constant α_s small, a study of the Regge limit is possible using perturbative quantum chromodynamics (QCD). The theoretical description is provided through the Balitsky-Fadin-Kuraev-Lipatov (BFKL) evolution, which achieves a resummation of perturbative higher order corrections, which are enhanced by a large logarithm in x to all orders in the strong coupling at leading (LL) [1–4] and next-to-leading (NLL) [5,6] logarithmic accuracy. Here $x = M^2/s$ where M denotes the characteristic hard scale of the process and s the center of mass energy squared. The perturbative high energy limit is then defined as $x \to 0$ at $M =$ fixed. BFKL evolution predicts a powerlike rise of the proton structure function F_2 with $1/x$, which is driven by the gluon distribution. While this rise is seen in the data and can be described by BFKL evolution [7–10], it is known that it cannot continue down to arbitrary small values of x. Instead, BFKL evolution will eventually drive the proton into an over occupied system of gluons, which eventually leads to the saturation of gluon densities [11]. Finding convincing and substantial evidence for gluon saturation as well as for the transition into this region of QCD phase space is still one of the open problems of QCD and at the core of the physics program of the future Electron Ion Collider [12].

A very useful observable to explore the gluon distribution at the LHC in this region of interest is provided by exclusive photo-production of vector mesons. The observable is somewhat complementary to the bulk of studies currently undertaken [13–21], which attempt to resolve the hadronic final state in order to explore the low x gluon. In contrast to those studies, exclusive photo-production of vector mesons allows for a direct observation of the energy dependence of the photo-production cross section which directly translates into the x-dependence of the underlying gluon distribution. In particular, if both HERA and LHC data are combined, the probed region in x extends over several orders of magnitude of x, down to smallest values of $x = 4 \times 10^{-6}$. Photo-production of bound states of charm quarks, *i.e.,* J/Ψ and $\Psi(2s)$ vector mesons, are then attractive observables, since the charm mass provides a hard scale at the border between soft and hard physics; the observable is therefore expected to be particularly sensitive to the possible presence of a semihard scale associated with the transition to the saturation region, the so-called saturation scale.

In [22] it has been found that an unintegrated gluon distribution subject to NLO BFKL evolution (the Hentschinski-Salas-Sabio Vera gluon; HSS) [7,8] is able to describe the energy dependence of the photo-production cross section of J/Ψ and Υ vector mesons. In [23], this

study has been extended to the Kutak-Sapeta (KS) gluon [24], which is subject to non-linear Balitsky-Kovchegov (BK) evolution [25,26]. While both gluon distributions were able to describe the available data set, we found that a certain perturbative expansion, which underlies the linear HSS gluon, leads to an instability at highest values of the center of mass energy W. While the instability can be removed through an improved scale setting, the growth of the stabilized gluon distribution with energy is too strong and linear evolution does no longer describe the dataset. This observation was then interpreted as a first indication for the transition toward saturated gluon densities. Note that in [27] is has been pointed out that this observation does not indicate saturation of gluon densities, but mainly the need for absorptive corrections (in the terminology of [27]). We agree in principle with this observation: the gluon does certainly not saturate at current values of the center of mass energy; one merely finds signs for the slow down of the powerlike growth which points toward an increasing relevance of nonlinear terms in low x QCD evolution equations. In other words, the cross section is about to enter the so-called transition region, which separates the phase space region characterized by low and saturated gluon densities respectively. For a related study based on a different implementation of BFKL evolution, see [28], also [29].

In the present paper we extend the study of [23], to the case of radially excited charm-anti charm states, i.e., the $\Psi(2s)$ vector meson. As for photo-production of J/Ψ, the hard scale is provided by the charm mass, placing us at the boundary between soft and hard physics. On the other hand, the dependence of the light-cone wave function on the dipole size differs for $\Psi(2s)$ and J/Ψ. We therefore expect to test with $\Psi(2s)$ photo-production a slightly different region in transverse momentum of the unintegrated gluon distribution. To increase the precision of our study we used instead of the previously implemented boosted Gaussian model for the vector meson wave function [30–32], a more refined description based on the numerical solution of the Schrödinger equation for the charm-anticharm state, provided in [33,34].

The outline of this paper is as follows: In Sec. II we provide the technical details of our theoretical description, in Sec. III we present the results of our numerical study and a comparison to data, while in Sec. IV we summarize our results and draw our conclusions.

II. THEORETICAL SETUP OF OUR STUDY

In the following we describe the framework on which our study is based, see also Fig. 1. We study the process

$$\gamma(q) + p(p) \to V(q') + p(p'), \tag{1}$$

where $V = J/\Psi, \psi(2S)$ while γ denotes a quasireal photon with virtuality $Q \to 0$; $W^2 = (q+p)^2$ is the squared

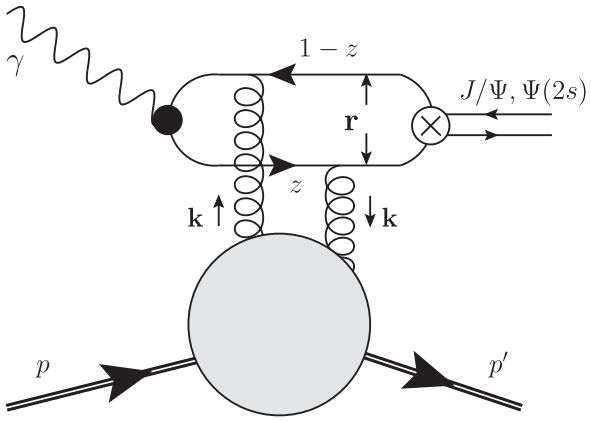

FIG. 1. Exclusive photo-production of vector mesons J/Psi and $\Psi(2s)$. For the quark-antiquark dipole we indicate photon momentum fractions z and $1-z$ as well as the transverse separation $\boldsymbol{r}$. Finally $\boldsymbol{k}$ denotes the transverse momentum transmitted from the unintegrated gluon distribution of the proton; the latter is indicated through the gray blob.

center-of-mass energy of the $\gamma(q) + p(p)$ collision. With the momentum transfer $t = (q-q')^2$, the differential cross section for the exclusive photo-production of a vector meson can be written in the following form

$$\frac{d\sigma}{dt}(\gamma p \to V p) = \frac{1}{16\pi} |\mathcal{A}_T^{\gamma p \to V p}(W^2, t)|^2. \tag{2}$$

where $\mathcal{A}_T(W^2, t)$ denotes the scattering amplitude for the reaction $\gamma p \to V p$ for color singlet exchange in the t-channel, with an overall factor W^2 already extracted. For a more detailed discussion see [22]. In the following we determine the total photo-production cross section, based on an inclusive gluon distribution. This is possible following a two step procedure, frequently employed in the literature: First one determines the differential cross section at zero momentum transfer $t = 0$ (which can be expressed in terms of the inclusive gluon distribution). In a second step the t-dependence is modeled, which then allows us to relate the differential cross section at $t = 0$ to the integrated cross section. In order to do so, we assume an exponential drop-off with $|t|$ of the differential cross section, $\sigma \sim \exp[-|t| B_D(W)]$ with an energy dependent t slope parameter B_D,

$$B_D(W) = \left[b_0 + 4\alpha' \ln \frac{W}{W_0} \right] \text{GeV}^{-2}. \tag{3}$$

The total cross section for vector meson production is therefore obtained as

$$\sigma^{\gamma p \to V p}(W^2) = \frac{1}{B_D(W)} \frac{d\sigma}{dt}(\gamma p \to V p)|_{t=0}. \tag{4}$$

The uncertainty introduced through the modeling of the t-dependence mainly affects the overall normalization of the

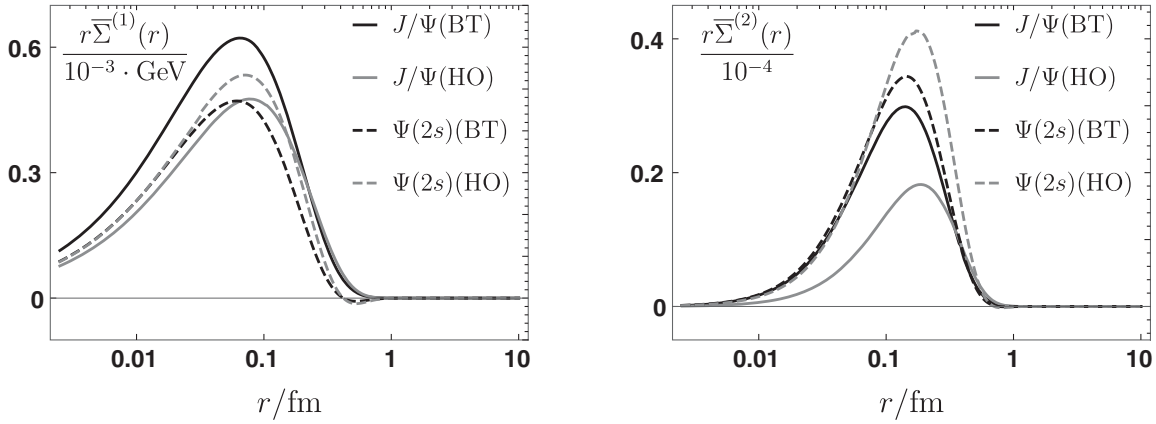

FIG. 2. The functions $\bar{\Sigma}_T^{(1)}$ (left) and $\bar{\Sigma}_T^{(2)}$ (right) as defined in Eq. (7) and multiplied with a factor of r for the Buchmüller-Tyle and harmonic oscillator potentials.

cross section with a mild logarithmic dependence on the energy. To determine the scattering amplitude, we first note that the dominant contribution is provided by its imaginary part. Corrections due to the real part of the scattering amplitude can be estimated using dispersion relations, in particular

$$\frac{\Re\mathrm{e}\mathcal{A}(W^2,t)}{\Im\mathrm{m}\mathcal{A}(W^2,t)}=\tan\frac{\lambda\pi}{2},\quad\text{with}\quad\lambda(x)=\frac{d\ln\Im\mathrm{m}\mathcal{A}(x,t)}{d\ln 1/x}. \tag{5}$$

As noted in [22], the dependence of the slope parameter λ on energy W provides a sizable correction to the W dependence of the complete cross section. We therefore do not assume $\lambda=$ const., but instead determine the slope λ directly from the W-dependent imaginary part of the scattering amplitude. To determine the latter, we go beyond the Gaussian model for the light-cone wave function of the vector mesons and use instead a refined description which includes relativistic spin-rotation effects. The imaginary part of the scattering amplitude is then in the forward limit obtained as [33–35]

$$\Im\mathrm{m}\mathcal{A}_T(W^2,t=0)=\int d^2\boldsymbol{r}\left[\sigma_{q\bar{q}}\left(\frac{M_V^2}{W^2},r\right)\bar{\Sigma}_T^{(1)}(r)+\frac{d\sigma_{q\bar{q}}(\frac{M_V^2}{W^2},r)}{dr}\bar{\Sigma}_T^{(2)}(r)\right], \tag{6}$$

with $r=|\boldsymbol{r}|$. The functions $\bar{\Sigma}_T^{(1,2)}$ describe the transition of a transverse polarized photon into a vector meson V and are given by [34]

$$\bar{\Sigma}_T^{(i)}(r)=\hat{e}_f\sqrt{\frac{\alpha_{e.m.}N_c}{2\pi^2}}K_0(m_f r)\Xi^{(i)}(r),\quad i=1,2 \tag{7}$$

where

$$\Xi^{(1)}(r)=\int_0^1 dz\int_0^\infty dp p J_0(p\cdot r)\times\frac{m_T^2+m_T m_L-2p^2z(1-z)}{m_T+m_L}\Psi_V(z,p),$$
$$\Xi^{(2)}(r)=\int_0^1 dz\int_0^\infty dp p^2 J_1(p\cdot r)\times\frac{m_T+m_L+m_T(1-2z)^2}{2m_T(m_T+m_L)}\Psi_V(z,p), \tag{8}$$

and $\hat{e}_f=2/3$ is the charge of the charm quark while $\alpha_{e.m.}$ the electromagnetic fine structure constant; $N_c=3$ denotes the number of colors and K_0 is a Bessel function of the second kind and $J_{0,1}$ a Bessel function of first kind. Finally, with m_f the mass of the charm quark, and $p=|\boldsymbol{p}|$ the modulus of the transverse momentum, we have

$$m_T^2=m_f^2+p^2\qquad m_L^2=4m_f^2z(1-z), \tag{9}$$

with $\Psi_V(z,p)$ the wave function of the vector meson. The latter has been obtained in [33,34] through the numerical solution of the Schrödinger equation for a given choice of the heavy quark interaction potential and provided in the boosted form as a table in both photon momentum fraction z and transverse momentum p. The above form includes both effects due to the so-called Melosh spin rotation as well as a more realistic r-dependence of the photon-vector meson transition, with which we convolute the dipole cross section $\sigma_{q\bar{q}}(x,r)$. The functions $\bar{\Sigma}^{(i)}$ are plotted against the dipole separation in Fig. 2. The central observations are the small, but visible node at $r\simeq 0.8$ fm for the $\Psi(2s)$ ($\bar{\Sigma}^{(1)}(r)$) and the relative enhancement of $\Psi(2s)$ with respect to the J/Ψ for $\bar{\Sigma}^{(2)}(r)$, which is particularly pronounced for the harmonic oscillator potential.

As in [23], we calculate in the following the dipole cross section from two underlying unintegrated gluon distributions $\mathcal{F}(x,\boldsymbol{k}^2)$, using the relation [36]

$$\sigma_{q\bar{q}}(x,r)=\frac{4\pi}{N_c}\int\frac{d^2\boldsymbol{k}}{\boldsymbol{k}^2}(1-e^{i\boldsymbol{k}\cdot\boldsymbol{r}})\alpha_s\mathcal{F}(x,\boldsymbol{k}^2). \quad (10)$$

Our study is based on two different implementations, the KS and HSS unintegrated gluon densities respectively:

(i) the KS gluon has been obtained as a solution of the momentum space version of the BK equation with modifications according to the Kwieciski-Martin-Stasto (KMS) prescription [37]. This implies an implementation of a so-called kinematical constraint, leading to energy momentum conservation, as well as complete DGLAP splitting functions, including quarks. In the collinear limit, the underlying evolution equation reduces therefore to the conventional DGLAP evolution. The KS gluon distribution in the proton was fitted [24] to proton structure function data measured at the HERA experiments H1 and ZEUS [38]. For a more detailed discussion see [24,37].

(ii) The HSS gluon is subject to NLO BFKL evolution, including a resummation of collinearly enhanced terms in the NLO BFKL kernel as well as a resummation of large running coupling corrections using the optimal scale setting procedure. The initial conditions have been fitted [7,8] to the same HERA data set as the KS gluon. For a more detailed discussion see [7,39].

While the HSS gluon provides a very good description of both Υ and J/Ψ photo-production data [22,23], it has been found in [23] that the perturbative expansion used for the solution of the NLO BFKL equation turns unstable at lowest values of x. In particular one finds at the level of the dipole cross section two terms

$$\sigma^{(\mathrm{HSS})}_{q\bar{q}}(x,r,M,\bar{M})=\sigma^{(\mathrm{dom.})}_{q\bar{q}}(x,r,M,\bar{M})+\sigma^{(\mathrm{corr.})}_{q\bar{q}}(x,r,M,\bar{M}), \quad (11)$$

where

$$\hat{\sigma}^{(\mathrm{dom})}_{q\bar{q}}(x,r,M,\bar{M})=\alpha_s(\bar{M}\cdot Q_0)\int_{\frac{1}{2}-i\infty}^{\frac{1}{2}+i\infty}\frac{d\gamma}{2\pi i}\left(\frac{4}{r^2Q_0^2}\right)^{\gamma}f(\gamma,\delta,r)\left(\frac{1}{x}\right)^{\chi(\gamma,M,\bar{M})}$$

$$\hat{\sigma}^{(\mathrm{corr.})}_{q\bar{q}}(x,r,M,\bar{M})=\alpha_s(\bar{M}\cdot Q_0)\int_{\frac{1}{2}-i\infty}^{\frac{1}{2}+i\infty}\frac{d\gamma}{2\pi i}\left(\frac{4}{r^2Q_0^2}\right)^{\gamma}f(\gamma,\delta,r)\left(\frac{1}{x}\right)^{\chi(\gamma,M,\bar{M})}\times\frac{\bar{\alpha}_s^2\beta_0\chi_0(\gamma)}{8N_c}\log\left(\frac{1}{x}\right)\left[-\psi(\delta-\gamma)+\log\frac{M^2r^2}{4}-\frac{1}{1-\gamma}-\psi(2-\gamma)-\psi(\gamma)\right], \quad (12)$$

and

$$f(\gamma,\delta,r)=\frac{r^2\cdot\mathcal{C}\pi\Gamma(\gamma)\Gamma(\delta-\gamma)}{N_c(1-\gamma)\Gamma(2-\gamma)\Gamma(\delta)}, \quad (13)$$

is a function which collects both factors resulting from the proton impact factor and the transformation of the unintegrated gluon density to the dipole cross section, see [7,22] for details. The parameters $Q_0=0.28$ GeV, $\mathcal{C}=2.29$ and $\delta=6.5$ have been determined from a fit to HERA data in [7]. $\chi(\gamma,M^2)$ is the next-to-leading logarithmic (NLL) BFKL kernel which includes a resummation of both collinear enhanced terms as well as a resummation of large terms proportional to the first coefficient of the QCD beta function, $\beta_0=11N_c/3-2n_f/3$ through the Brodsky-Lepage-Mackenzie (BLM) optimal scale setting scheme [40], with $N_c=3$ and $n_f=4$ the number of colors and active flavors respectively. This procedure yields then in turn a γ-dependent running coupling constant, $\bar{\alpha}_s=\alpha_s^{\mathrm{BLM}}(\bar{M}\cdot Q_0,\gamma)N_c/\pi$, see [7,8] for details. Running couplings constants are evaluated at $n_f=4$ with $\Lambda_{\mathrm{QCD}}=0.21$ GeV, see [7,8] for details. The NLL kernel with collinear improvements reads

$$\chi(\gamma,M,\bar{M})=\bar{\alpha}_s\chi_0(\gamma)+\bar{\alpha}_s^2\tilde{\chi}_1(\gamma)-\frac{1}{2}\bar{\alpha}_s^2\chi_0'(\gamma)\chi_0(\gamma)+\chi_{\mathrm{RG}}(\bar{\alpha}_s,\gamma,\tilde{a},\tilde{b})-\frac{\bar{\alpha}_s^2}{8N_c}\chi_0(\gamma)\log\frac{\bar{M}^2}{M^2}. \quad (14)$$

where χ_i, $i=0,\ 1$ denotes the LO and NLO BFKL eigenvalue and χ_{RG} resums (anti-)collinear poles to all orders; for details about the individual kernels see [7,22]. The scale M is a characteristic hard scale of the process, while $\bar{M}$ sets the scale of the running coupling constant, see [7,22] for details. As in [22] we consider here the possibility that—unlike in the original fit—that $\bar{M}\neq M$ which we use to estimate the uncertainty in the energy dependence the obtained dipole cross section. The term $\sigma^{\mathrm{corr.}}$ contains running coupling corrections related to the transverse momentum dependence of external particles which do not exponentiate. They have been therefore treated in [7] as a perturbative correction to the BFKL Green's function. Even though $\sigma^{\mathrm{corr.}}$ is suppressed by a relative factor of α_s^2, enhancement by $\ln(1/x)$ will eventually compensate for the smallness of the strong coupling constant and invalidate the perturbative expansion which in turn gives rise to the aforementioned instability. In [23] it has been found that this instability can be cured through adopting a scale setting, similar to those used in fits of the so-called IP-sat model [41,42], through choosing $M^2=\frac{4}{r^2}+\mu_0^2$ with $\mu_0^2=1.51\ \mathrm{GeV}^2$. It is important to note that this change in the hard scale—even though well motivated—yields a dipole cross section which does no longer fit the very precise HERA data; in particular the overall normalization requires an adjustment. The resulting dipole distribution provides an opportunity to explore

stabilized perturbative NLO BFKL evolution for the description of exclusive vector meson photon production, while the parameters Q_0 and δ could in principle still be further adjusted. We will not make use of this possibility in this study. In the following we will distinguish the two possible implementation of the HSS dipole cross section as "fixed" and "dipole" scale respectively.

III. RESULTS

For our study we make use of two sets of vector meson wave functions provided by the authors of [33,34]. They are based on a numerical solution of the Schrödinger equation with harmonic oscillator (HO) and Buchmüller-Tye potential [43] respectively which has been performed and is provided by the authors of [33,34]; we refer also to these references for a compact summary of the precise form of the underlying charm-anticharm potentials. While the Buchmüller-Tye potential uses a charm mass of $m_f = 1.48$ GeV, the harmonic oscillator potential is associated with a charm mass of $m_f = 1.4$ GeV. For the parameters of the diffractive slope B_D, defined in Eq. (3), we use the following parameters which have been determined in [34] from a fit to HERA data:

$$b_0^{(J/\Psi)} = 4.62, \qquad b_0^{\Psi(2s)} = b_0^{(J/\Psi)} + 0.24,$$
$$\alpha'_{J/\Psi}(0) = 0.171, \qquad \alpha'_{\Psi(2s)}(0) = \alpha'_{J/\Psi}(0) - 0.02. \tag{15}$$

In agreement with the original fits of the KS gluon, the overall strong coupling constant which arises from Eq. (11) is evaluated at the charm mass for the KS gluon with $\alpha_s(m_c) = 0.31$. In the case of the HSS gluon, this coupling constant is evaluated following Eq. (12). The results of our study for the J/Ψ cross section are shown in Fig. 3, for the $\Psi(2s)$ in Fig. 4. To estimate uncertainties associated with the low x evolution, we vary for the HSS gluon the hard scale in the range $M \to M/2, 2 \cdot M$. For both KS and HSS gluon the following statement applies: Since the cross section is proportional to the square of the strong coupling constant, the overall normalization is strongly dependent on the value of the overall coupling constant. Moreover, due to the absence of next-to-leading order corrections for the photon-vector meson impact factor, the value of this coupling is not well constrained and leads to a significant scale uncertainty, and can easily yield changes in the normalization in the range of an overall factor of 0.51 up to 1.65. Moreover in [33,34] a strong dependence of the normalization of the photon-vector meson impact factor on the model dependent value of the charm mass has been found. Further uncertainties in the overall normalization arise due to the absence of the so-called skewness corrections, see [44,45]. As pointed out in [22], we believe that it is not clear whether the approximations used in [44,45] are appropriate for the current setup based on high energy factorization, see also the related discussion

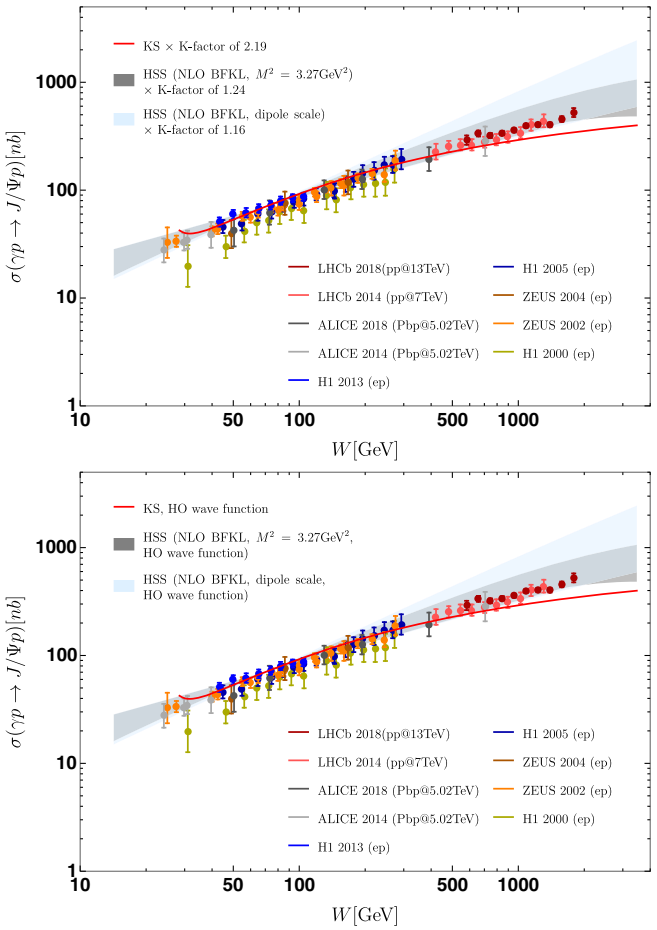

FIG. 3. Energy dependence of the J/Ψ photo-production cross section as provided by the KS and HSS gluon distribution (see text). The shaded regions correspond to a variation of the scale $\bar{M} \to \{\bar{M}/2, \bar{M}2\}$. The upper/lower plot uses J/Ψ wave functions based on the Buchmüller-Tyle and harmonic oscillator potential respectively. We further display photo-production data measured at HERA by ZEUS [48,49] and H1 [46,50,51] as well as LHC data obtained from ALICE [52,53] and LHCb (W^+ solutions) [54,55] collaborations.

in [34]. We therefore do not include a skewness factor. Nevertheless, the skewness correction of [44,45] would yield in our case with the given values for the effective intercept λ, see Eq. (5), a correction in the overall normalization which ranges between a factor 0.872 and 1.53. To separate this normalization uncertainty from the uncertainty associated with the description of the energy dependence, on which we focus in this paper, we fit in the following the overall normalization of our theory prediction to low energy H1 data for J/Ψ photo-production [46] (with $W/\text{GeV}^2 \in [43.2, 104.2]$) and the ratio of $\Psi(2s)$ and J/Ψ cross section [47] (with $W/\text{GeV}^2 \in [53.2, 128.3]$). We chose here the ratio of $\Psi(2s)$ and J/Ψ cross section, as a reference since to the best of our knowledge these the only published and independently determined low energy

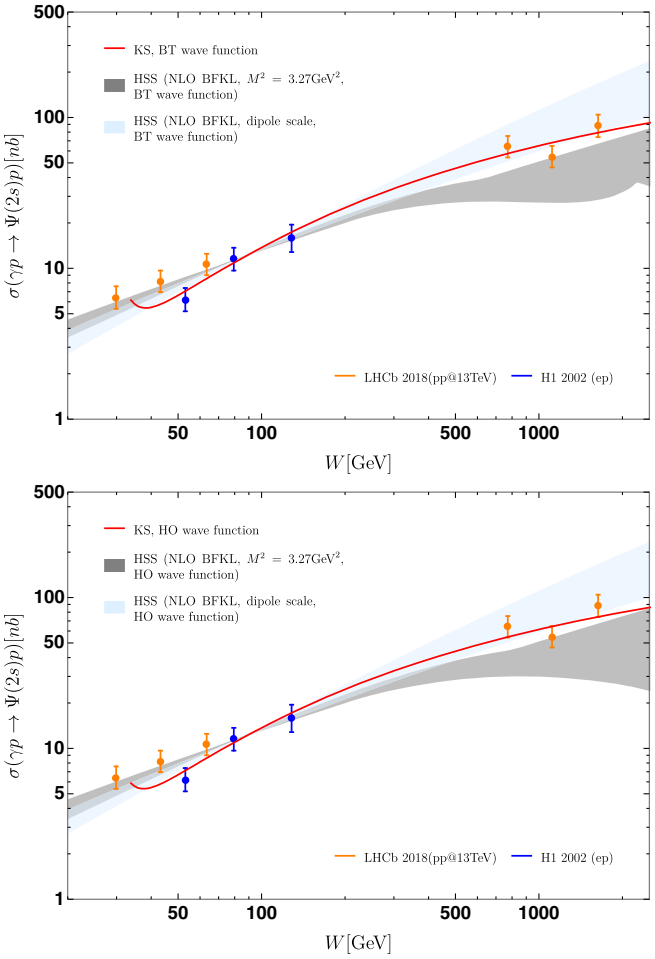

FIG. 4. Energy dependence of the $\Psi(2s)$ photo-production cross section as provided by the KS and HSS gluon distribution (see text). The shaded regions correspond to a variation of the scale $\bar{M} \to \{\bar{M}/2, \bar{M}2\}$. The upper/lower plot uses the wave function based on the Buchmüller-Tyle and harmonic oscillator potential respectively. We further display photo-production data measured at HERA by the H1 [47,56] as well as LHC data obtained from the LHCb collaboration (W^+ and W^- solutions) [55].

data for $\Psi(2s)$ photo-production, which are currently available. Note that we do not only make such an adjustment for different versions of the KS and HSS gluon, but we also adjust separately the overall normalization if we vary the renormalization scale of the HSS gluon in the range $M \to M/2, 2M$. In this way our uncertainty bands shows only the uncertainty in the low x evolution and not in the overall normalization, which is easily twice as big. The shown predictions are therefore obtained through Eq. (4) which is then multiplied by the adjusted normalization factors, collected in Table I. In some cases these adjustments in the overall normalization are rather large and can reach values of up to 2.19. Nevertheless, given the uncertainties in the overall normalization listed above, these values have a natural explanation and are therefore reasonable within the current limitations of the description.

TABLE I. Results of the re-fit of the overall normalization to H1 J/Ψ data [46] with $W/\text{GeV} \in [43.2, 104.2]$ and H1 data for the $\Psi(2s) - J/\Psi$ ratio [47] with $W/\text{GeV} \in [53.2, 128.3]$. Values for $\Psi(2s)$ are calculated as a product of the normalization of ratio and J/Psi.

	KS	HSS (dipole scale, BT)			HSS (fixed scale, BT)		
	(BT)	$M/2$	M	$2M$	$M/2$	M	$2M$
J/Ψ	2.17	1.92	1.36	1.36	1.91	1.23	1.25
ratio	0.74	0.92	1.10	1.06	0.68	0.94	0.99
$\Psi(2s)$	1.60	1.76	1.49	1.44	1.30	1.16	1.24

	KS	HSS (dipole scale, HO)			HSS (fixed scale, HO)		
	(HO)	$M/2$	M	$2M$	$M/2$	M	$2M$
J/Ψ	2.19	1.81	1.24	1.25	1.94	1.16	1.16
ratio	0.41	0.56	0.67	0.65	0.39	0.57	0.61
$\Psi(2s)$	0.92	1.01	0.83	0.81	0.74	0.66	0.71

For the description of the energy dependence of J/Ψ photo-production, Fig. 3, we confirm the observation made in [23]: the fixed scale BFKL dipole follows the nonlinear KS gluon, which can be explained due to previously mentioned instability of this solution at largest values of W. Nevertheless, the uncertainty band associated with the dipole scale HSS gluon does no longer allow to clearly discard this solution through the data. Indeed, the nonlinear KS gluon seems to slightly undershoot the data at highest W-values and therefore can be no longer identified as the preferred description. In addition, similar to the case of the HSS gluon, one should also associate with the KS gluon an uncertainty band, which we estimate to be similar in magnitude or even larger than the one of the HSS gluon. At the same time it should be stressed that the error bars shown for the LHCb data at highest values of W reflect only the error associated with the hadronic cross sections and uncertainties due to the extraction of the photon-proton cross section are not included. It is therefore likely that these error bars do not reflect the complete uncertainty associated with these data points. We therefore conclude that it is not possible to clearly identify one of the two gluons as the appropriate description of the currently available J/Ψ dataset.

The situation is even less clear if we turn to the $\Psi(2s)$ photo-production cross section Fig. 4. While the dipole scale HSS gluon and the KS gluon both provide a very good description of the energy dependence with essentially identical result for the wave function based on Buchmüller-Tyle and harmonic oscillator potential, the consequences of the instability of the fixed scale HSS gluon are even more severe in this case. Indeed, starting with $W > 780$ GeV (BT wave function) and

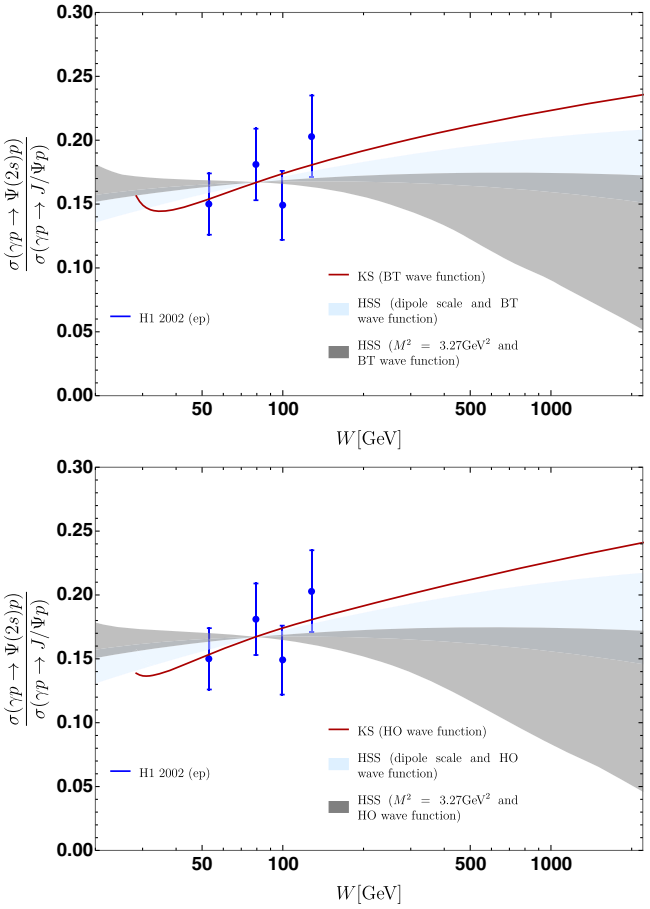

FIG. 5. Energy dependence of the ratio of $\Psi(2s)$ vs J/Ψ photo-production cross section as provided by the KS and HSS gluon distributions for both Buchmüller-Tye (BT) and harmonic oscillator (HO) vector meson wave functions. The shaded regions correspond to a variation of the scale $\bar{M} \to \{\bar{M}/2, \bar{M}2\}$ with the normalization for each scale setting individually fixed through a fit to H1 data, see Table I. We further display photo-production data measured at HERA by the H1 collaboration [47].

$W > 880$ GeV some of the solutions explored within the uncertainty band develop a negative intercept λ, see Eq. (5), and solutions associated with lower and upper limits of the scale variations start to cross. For $x < 3.50 \times 10^{-6}$, corresponding to $W > 1970$ GeV, we find values of $\lambda < -0.5$, and we clearly leave the region of applicability of Eq. (5) to determine the real part through the imaginary part. Indeed, Eq. (5) suggests in this case that the subleading real part would be larger (with respect to its absolute value) than the corresponding imaginary part. For center of mass energies $W > 3.5$ TeV (not shown) one eventually reaches values $\lambda < -1$ and the description breaks down completely. A few details on the origin of this instability of the fixed order description in the case of $\Psi(2s)$ production are collected in the Appendix, which explain the origin of this instability both in terms of the perturbative expansion underlying Eq. (11) and the particular structure of the $\Psi(2s)$ wave function.

While both the J/Ψ and $\Psi(2s)$ photo-production cross section can currently not distinguish between linear and nonlinear QCD evolution, we make an interesting observation if we consider instead the ratio of both cross section, Fig. 5. We find that the KS gluon, subject to nonlinear BK evolution, and the dipole scale HSS gluon, subject to linear NLO evolution, predict a different energy dependence for the ratio of $\Psi(2s)$ and J/Ψ photo-production cross sections. While linear NLO BFKL evolution predicts a ratio which is approximately constant with energy, non-linear KS evolution predicts an increase with energy of the cross section ratio. While the uncertainty of the HSS fixed scale solution is large and should be considered with care, given the existing problems in the description of the $\Psi(2s)$ photo-production cross section, this ratio seems to decrease with energy in this case. In particular, while the fixed scale HSS gluon and the KS gluon give very similar predictions for the J/Ψ photo-production cross section, the corresponding predictions are rather different for the ratio. We believe that this observation can be useful for two reasons: First of all it is well known that uncertainties are generally reduced for such cross section ratios. This refers both to the aforementioned skewness factor as well as to the extraction of the photo-production cross section from hadronic data, which requires to control the so-called rapidity gap survival probability. Second, while the differences between linear and nonlinear evolution are in general not large at current center-of-mass energies, they seem to follow a different tendency, i.e., the cross section ratio increases for nonlinear evolution and decreases for linear evolution. Moreover, linear predictions which mimic the energy dependence of the nonlinear gluon through a perturbative instability lead—at least in the present case—to a very different energy dependence for the ratio. As far as data are concerned, we find that H1 data seem to prefer a rise of the ratio with energy. Nevertheless, due to the relative large error bars as well as their limitation to the region $W = 50$–110 GeV, the H1 data set is in complete agreement with both linear and non-linear evolution. LHCb data, which would cover the region of large energies W, are currently only provided for J/Ψ and $\Psi(2s)$ photo-production cross sections separately. While it is in principle possible to take ratios of these results, the published W-bins of J/Ψ and $\Psi(2s)$ cross sections differ, which complicates a proper extraction of the cross section ratio. We however believe that it would be very interesting to compare in the future our predictions to properly extracted cross section ratios. In particular, regardless of still sizeable theoretical uncertainties, it would be interesting to see whether experimental data indicate a rising or falling ratio with energy.

IV. CONCLUSION

In this paper we extended previous studies, dedicated to the study of the energy dependence of the exclusive J/Ψ photo-production cross section to $\Psi(2s)$ vector mesons.

We furthermore used a more accurate description of the photon to vector meson transition, as provided by [33,34], as well as a refined discussion of the theoretical uncertainties of the energy dependence of the linear HSS gluon. Reconsidering J/Ψ photo-production including the above mentioned improvements, we find that we cannot completely confirm the claim made in [23]. Linear, stabilized HSS evolution, based on the dipole scale setting and nonlinear KS evolution differ for largest scattering energies W, but the difference is not big enough such that current LHC data can unambiguously distinguish between one of the two QCD evolution equations, in particular once uncertainties of the HSS gluon are included. While the difference between HSS gluon with dipole scale setting and KS gluon is even less pronounced for $\Psi(2s)$ photo-production, we find that the HSS gluon with fixed scale suffers a more pronounced instability than observed previously for the J/Ψ. While, given the current uncertainties in the theory description, the energy dependence of J/Ψ and $\Psi(2s)$ seems at current energies not to allow to distinguish between linear and nonlinear evolution equations, we find it encouraging that the ratio of J/Ψ and $\Psi(2s)$ photo-production cross section shows a different energy behavior for linear and nonlinear evolution. In this context we would like to stress that a similar observation has been already made in [34]: with the gluon modeled through the phenomenological KST dipole cross section [57], an increase of the ratio with energy has been found. At the same time, an almost constant ratio has been found for the ratio of $\Upsilon(2s)$ and $\Upsilon(1s)$ photo-production cross section which are both placed well in the perturbative region due to the hard scale provided by the bottom quark mass. The current study goes beyond this observation, since our gluon distributions are obtained as the solution to low x QCD evolution equations and are both obtained at a hard scale of the order of the charm mass.

From the theory side it is necessary to further increase the accuracy of predictions for photo-production cross sections, in particular the rather large adjustment in the overall normalization, see Table I. While there are various sources of uncertainty, one may at least expect to reduce the uncertainty in the overall normalization due to a determination of next-to-leading order perturbative corrections to the photon-to-vector meson impact factor, see [58–61] for past and recent efforts in this direction. Despite of the theoretical uncertainties, we believe that a precise extraction of the ratio of $\Psi(2s)$ and J/Ψ photo-production cross sections could be very useful to distinguish in the future between linear and nonlinear QCD evolution. We believe that this applies both to photon-proton scattering at highest center of mass energies as measured at LHC, as well as for photo-production cross sections obtained in electron-ion scattering at the future Electron Ion Collider. While in the latter case, center-of-mass energies will be naturally lower, nuclear effects will likely enhance gluon densities and therefore the possible relevance of nonlinear QCD evolution.

ACKNOWLEDGMENTS

Support by Consejo Nacional de Ciencia y Tecnología Grant No. A1 S-43940 (CONACYT-SEP Ciencias Básicas) is gratefully acknowledged. We further would like to thank Andrés Nieto Betanzos for collaboration at an early stage of this project.

APPENDIX: DETAILS ON THE BFKL DESCRIPTION WITH FIXED SCALE

In this Appendix we provide some details on the instability of the fixed scale HSS gluon for $\Psi(2s)$ photo-production. As already pointed out in [23] and also discussed in Sec. II, the decomposition of the BFKL Green's function into two terms leads to an instability of the dipole cross section at relatively low hard scales and high center of mass energies. Since the second term in Eq. (11) is negative and growing in magnitude with energy, one finds obtains, due to the presence of a logarithm in dipole size, a characteristic dip around $r = 0.05$ fm appears, which leads for $x < 10^{-3}$ to a region of negative dipole cross sections which grows with decreasing x, see [23] for a detailed discussion. If convoluted with the photon-to-J/Ψ impact factor this negative region leads in turn to a slow down of the growth with energy of the scattering amplitude, at least within the range of energies W accessible at LHC. To illustrate this effect, we provide in Fig. 6 the product of photon-to-J/Ψ transition multiplied with the fixed scale HSS dipole cross section against the dipole size for different values of $x = M_V^2/W^2$; for comparison we further show the dipole size scale HSS case. For lowest values of x, the negative contribution is sizeable in the case of the fixed scale solution. Nevertheless, after convolution of the HSS dipole with fixed scale with the $\Sigma^{(1)}$ at a typical low x value of at $x = 0.4 \times 10^{-5}$, we still reach 59.8% of the corresponding expression obtained with the HSS dipole evaluated at a dipole size scale. Albeit the effect of the negative region clearly affects the theoretical prediction in this region, a description of data is still possible within the provided uncertainty bands.

In the case of the photon-to-$\Psi(2s)$ transition, one finds two such effects: (a) a negative region in the photon-to-$\Psi(2s)$ transition at $r \simeq 0.8$ fm due to the presence of a node in the $\Psi(2s)$ wave function, see also Fig. 2, and the dip region at $r \simeq 0.05$ fm in the case of the fixed scale HSS solution. Note that the presence of this node is of particular importance for non-saturated gluons, since the latter typical grow with dipole size r. This leads to an enhancement of this region with respect to a saturated gluon, which approaches a constant value for large values of r. The corresponding integrands are shown in Fig. 7. While in the case of the dipole size scale HSS gluon, the negative

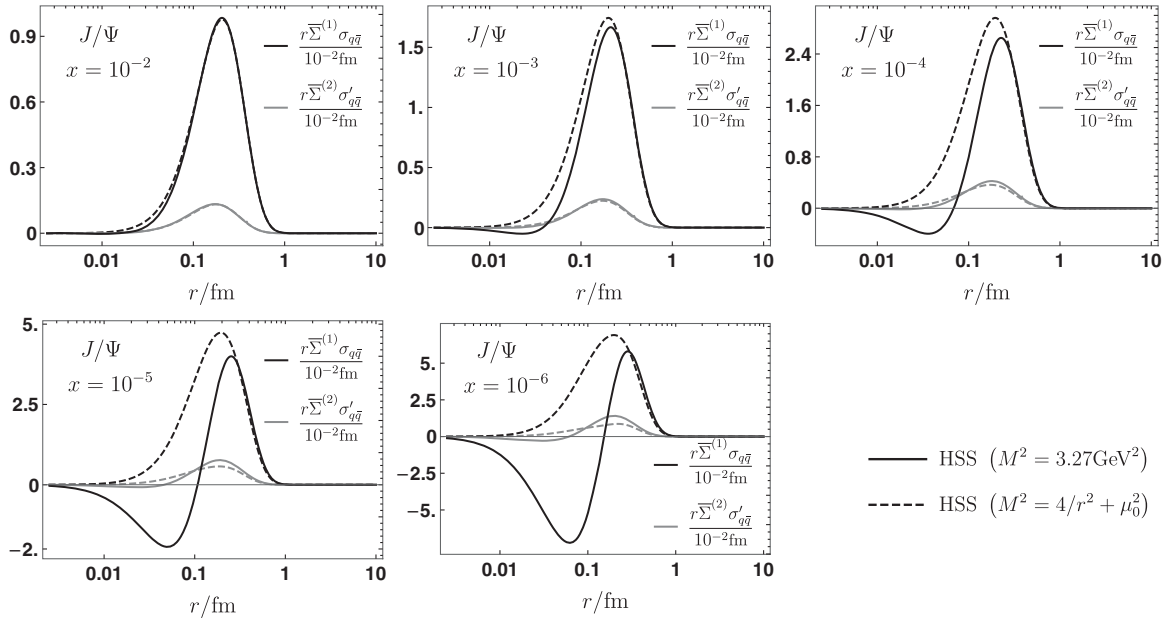

FIG. 6. Overlap of photon to J/Ψ transition light-front wave function and dipole cross section at different values of x. Solid lines correspond to the HSS gluon with fixed external renormalization scale, dashed lines to the dipole size dependent renormalization scale. For this comparison we use the Buchmüller-Tye wave function.

contribution due to the node at is compensated by the positive contributions at $r \simeq 0.1$ fm, the dipole cross section itself turns negative at such values of r for the fixed scale HSS gluon. The combination of both effects leads then to an even stronger reduction of the scattering amplitude with x, since both negative regions increase with energy. As a consequence, the ratio of fixed scale HSS gluon, convoluted with $\Sigma^{(1)}$, and the corresponding expression based on the dipole size scale HSS dipole amounts now only to 14.6% at $x = 0.4 \times 10^{-5}$. Moreover, the characteristic growth of the BFKL gluon with energy is reversed and the scattering amplitude starts to decrease with energy, already in the region of energies W accessible at LHC.

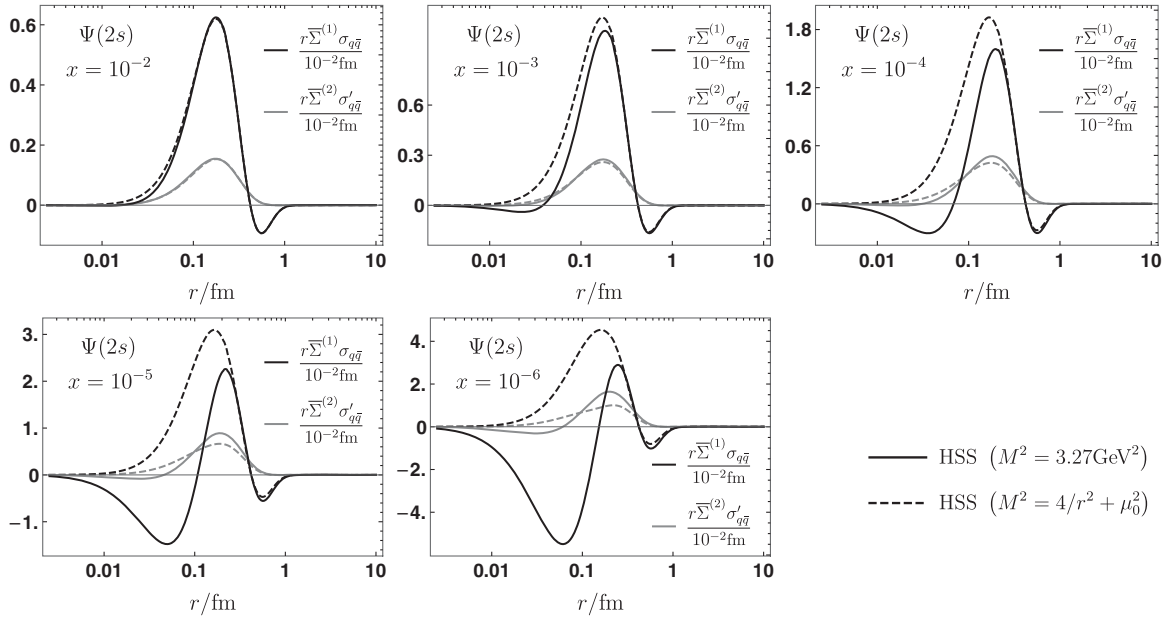

FIG. 7. Overlap of the photon to $\Psi(2s)$ transition light-front wave function and dipole cross section at different values of x. Solid lines correspond to the HSS gluon with fixed external renormalization scale, dashed lines to the dipole size dependent renormalization scale. For this comparison we use the Buchmüller-Tye wave function.

[1] E. A. Kuraev, L. N. Lipatov, and V. S. Fadin, Multi—Reggeon processes in the Yang-Mills theory, Sov. Phys. JETP **44**, 443 (1976).

[2] L. N. Lipatov, Reggeization of the vector meson and the vacuum singularity in nonabelian gauge theories, Sov. J. Nucl. Phys. **23**, 338 (1976).

[3] E. A. Kuraev, L. N. Lipatov, and V. S. Fadin, The Pomeranchuk singularity in nonabelian gauge theories, Sov. Phys. JETP **45**, 199 (1977).

[4] I. I. Balitsky and L. N. Lipatov, The Pomeranchuk singularity in quantum chromodynamics, Sov. J. Nucl. Phys. **28**, 822 (1978).

[5] V. S. Fadin and L. N. Lipatov, BFKL pomeron in the next-to-leading approximation, Phys. Lett. B **429**, 127 (1998).

[6] M. Ciafaloni and G. Camici, Energy scale(s) and next-to-leading BFKL equation, Phys. Lett. B **430**, 349 (1998).

[7] M. Hentschinski, A. Sabio Vera, and C. Salas, Hard to Soft Pomeron Transition in Small-x Deep Inelastic Scattering Data Using Optimal Renormalization, Phys. Rev. Lett. **110**, 041601 (2013).

[8] M. Hentschinski, A. Sabio Vera, and C. Salas, F_2 and F_L at small x using a collinearly improved BFKL resummation, Phys. Rev. D **87**, 076005 (2013).

[9] H. Kowalski, L. N. Lipatov, D. A. Ross, and O. Schulz, Decoupling of the leading contribution in the discrete BFKL analysis of high-precision HERA data, Eur. Phys. J. C **77**, 777 (2017).

[10] H. Kowalski, L. N. Lipatov, D. A. Ross, and G. Watt, Using HERA data to determine the infrared behaviour of the BFKL amplitude, Eur. Phys. J. C **70**, 983 (2010).

[11] L. V. Gribov, E. M. Levin, and M. G. Ryskin, Semihard processes in QCD, Phys. Rep. **100**, 1 (1983).

[12] A. Accardi, J. L. Albacete, M. Anselmino, N. Armesto, E. C. Aschenauer, A. Bacchetta, D. Boer, W. K. Brooks, T. Burton, N. B. Chang *et al.*, Electron ion collider: The next QCD frontier: Understanding the glue that binds us all, Eur. Phys. J. A **52**, 268 (2016).

[13] M. Bury, A. van Hameren, P. Kotko, and K. Kutak, Forward trijet production in p-p and p-Pb collisions at LHC, J. High Energy Phys. 09 (2020) 175.

[14] A. van Hameren, P. Kotko, K. Kutak, and S. Sapeta, Broadening and saturation effects in dijet azimuthal correlations in p-p and p-Pb collisions at $\sqrt{s} = 5.02$ TeV, Phys. Lett. B **795**, 511 (2019).

[15] I. Kolbé, K. Roy, F. Salazar, B. Schenke, and R. Venugopalan, Inclusive prompt photon-jet correlations as a probe of gluon saturation in electron-nucleus scattering at small x, J. High Energy Phys. 01 (2021) 052.

[16] H. Mäntysaari, N. Mueller, F. Salazar, and B. Schenke, Multigluon Correlations and Evidence of Saturation from Dijet Measurements at an Electron-Ion Collider, Phys. Rev. Lett. **124**, 112301 (2020).

[17] T. Altinoluk, R. Boussarie, C. Marquet, and P. Taels, Photoproduction of three jets in the CGC: Gluon TMDs and dilute limit, J. High Energy Phys. 07 (2020) 143.

[18] F. G. Celiberto, D. Y. Ivanov, and A. Papa, Diffractive production of Λ hyperons in the high-energy limit of strong interactions, Phys. Rev. D **102**, 094019 (2020).

[19] F. G. Celiberto, D. Y. Ivanov, M. M. A. Mohammed, and A. Papa, High-energy resummed distributions for the inclusive Higgs-plus-jet production at the LHC, arXiv:2008.00501.

[20] A. D. Bolognino, F. G. Celiberto, M. Fucilla, D. Y. Ivanov, and A. Papa, High-energy resummation in heavy-quark pair hadroproduction, Eur. Phys. J. C **79**, 939 (2019).

[21] F. G. Celiberto, D. Gordo Gómez, and A. Sabio Vera, Forward Drell–Yan production at the LHC in the BFKL formalism with collinear corrections, Phys. Lett. B **786**, 201 (2018).

[22] I. Bautista, A. Fernandez Tellez, and M. Hentschinski, BFKL evolution and the growth with energy of exclusive J/ψ and Υ photoproduction cross sections, Phys. Rev. D **94**, 054002 (2016).

[23] A. Arroyo Garcia, M. Hentschinski, and K. Kutak, QCD evolution based evidence for the onset of gluon saturation in exclusive photo-production of vector mesons, Phys. Lett. B **795**, 569 (2019).

[24] K. Kutak and S. Sapeta, Gluon saturation in dijet production in p-Pb collisions at large hadron collider, Phys. Rev. D **86**, 094043 (2012).

[25] I. Balitsky, Operator expansion for high-energy scattering, Nucl. Phys. **B463**, 99 (1996).

[26] Y. V. Kovchegov, Small x F(2) structure function of a nucleus including multiple pomeron exchanges, Phys. Rev. D **60**, 034008 (1999).

[27] C. A. Flett, A. D. Martin, M. G. Ryskin, and T. Teubner, Very low x gluon density determined by LHCb exclusive J/ψ data, Phys. Rev. D **102**, 114021 (2020).

[28] V. P. Goncalves, D. E. Martins, and C. R. Sena, Exclusive vector meson production in electron—ion collisions at the EIC, LHeC and FCC–eh, Nucl. Phys. **A1004**, 122055 (2020).

[29] V. P. Goncalves, C. E. Krumreich, and W. K. Sauter, Exclusive vector meson photoproduction at high energies using the discrete BFKL approach, Int. J. Mod. Phys. A **35**, 2050057 (2020).

[30] S. J. Brodsky, T. Huang, and G. P. Lepage, The hadronic wave function in quantum chromodynamics, Report No. SLAC-PUB-2540, Stanford Linear Accelerator Center, 1980, https://www.slac.stanford.edu/pubs/slacpubs/2500/slac-pub-2540.pdf.

[31] J. Nemchik, N. N. Nikolaev, and B. G. Zakharov, Scanning the BFKL pomeron in elastic production of vector mesons at HERA, Phys. Lett. B **341**, 228 (1994).

[32] B. E. Cox, J. R. Forshaw, and R. Sandapen, Diffractive upsilon production at the LHC, J. High Energy Phys. 06 (2009) 034.

[33] M. Krelina, J. Nemchik, R. Pasechnik, and J. Cepila, Spin rotation effects in diffractive electroproduction of heavy quarkonia, Eur. Phys. J. C **79**, 154 (2019).

[34] J. Cepila, J. Nemchik, M. Krelina, and R. Pasechnik, Theoretical uncertainties in exclusive electroproduction of S-wave heavy quarkonia, Eur. Phys. J. C **79**, 495 (2019).

[35] J. Hufner, Y. P. Ivanov, B. Z. Kopeliovich, and A. V. Tarasov, Photoproduction of charmonia and total charmonium proton cross-sections, Phys. Rev. D **62**, 094022 (2000).

[36] M. Braun, Structure function of the nucleus in the perturbative QCD with $N_c \to \infty$ infinity (BFKL pomeron fan diagrams), Eur. Phys. J. C **16**, 337 (2000).
[37] J. Kwiecinski, A. D. Martin, and A. M. Stasto, A unified BFKL and GLAP description of F2 data, Phys. Rev. D **56**, 3991 (1997).
[38] F. D. Aaron *et al.* (H1 and ZEUS Collaborations), Combined Measurement and QCD Analysis of the Inclusive $e+-$ p scattering cross sections at HERA, J. High Energy Phys. 01 (2010) 109.
[39] G. Chachamis, M. Deák, M. Hentschinski, G. Rodrigo, and A. Sabio Vera, Single bottom quark production in $k_\perp$-factorisation, J. High Energy Phys. 09 (2015) 123.
[40] S. J. Brodsky, G. P. Lepage, and P. B. Mackenzie, On the elimination of scale ambiguities in perturbative quantum chromodynamics, Phys. Rev. D **28**, 228 (1983).
[41] A. H. Rezaeian, M. Siddikov, M. Van de Klundert, and R. Venugopalan, Analysis of combined HERA data in the impact-parameter dependent saturation model, Phys. Rev. D **87**, 034002 (2013).
[42] J. Bartels, K. J. Golec-Biernat, and H. Kowalski, A modification of the saturation model: DGLAP evolution, Phys. Rev. D **66**, 014001 (2002).
[43] W. Buchmuller and S. H. H. Tye, Quarkonia and quantum chromodynamics, Phys. Rev. D **24**, 132 (1981).
[44] A. G. Shuvaev, K. J. Golec-Biernat, A. D. Martin, and M. G. Ryskin, Off diagonal distributions fixed by diagonal partons at small x and xi, Phys. Rev. D **60**, 014015 (1999).
[45] A. D. Martin, M. G. Ryskin, and T. Teubner, $Q2$ dependence of diffractive vector meson electroproduction, Phys. Rev. D **62**, 014022 (2000).
[46] C. Alexa *et al.* (H1 Collaboration), Elastic and proton-dissociative photoproduction of $J/$psi mesons at HERA, Eur. Phys. J. C **73**, 2466 (2013).
[47] C. Adloff *et al.* (H1 Collaboration), Diffractive photoproduction of psi(2S) mesons at HERA, Phys. Lett. B **541**, 251 (2002).
[48] S. Chekanov *et al.* (ZEUS Collaboration), Exclusive photoproduction of $J/$psi mesons at HERA, Eur. Phys. J. C **24**, 345 (2002).
[49] S. Chekanov *et al.* (ZEUS Collaboration), Exclusive electroproduction of $J/$psi mesons at HERA, Nucl. Phys. **B695**, 3 (2004).
[50] A. Aktas *et al.* (H1 Collaboration), Elastic $J/$psi production at HERA, Eur. Phys. J. C **46**, 585 (2006).
[51] C. Adloff *et al.* (H1 Collaboration), Elastic photoproduction of $J/$psi and Upsilon mesons at HERA, Phys. Lett. B **483**, 23 (2000).
[52] B. B. Abelev *et al.* (ALICE Collaboration), Exclusive J/ψ Photoproduction off Protons in Ultra-Peripheral p-Pb Collisions at $\sqrt{s_{\rm NN}} = 5.02$ TeV, Phys. Rev. Lett. **113**, 232504 (2014).
[53] S. Acharya *et al.* (ALICE Collaboration), Energy dependence of exclusive J/ψ photoproduction off protons in ultra-peripheral p–Pb collisions at $\sqrt{s_{NN}} = 5.02$ TeV, Eur. Phys. J. C **79**, 402 (2019).
[54] R. Aaij *et al.* (LHCb Collaboration), Exclusive J/ψ and $\psi(2S)$ production in pp collisions at $\sqrt{s} = 7$ TeV, J. Phys. G **40**, 045001 (2013).
[55] R. Aaij *et al.* (LHCb Collaboration), Central exclusive production of J/ψ and $\psi(2S)$ mesons in pp collisions at $\sqrt{s} = 13$ TeV, J. High Energy Phys. 10 (2018) 167.
[56] D. Schmidt, Diffractive photoproduction of charmonium in the H1 detector at HERA, Report No. DESY-THESIS-2001-029, Hamburg University, 2001, https://inspirehep.net/files/01235a34aa443183445518ca96c82395.
[57] B. Z. Kopeliovich, A. Schafer, and A. V. Tarasov, Nonperturbative effects in gluon radiation and photoproduction of quark pairs, Phys. Rev. D **62**, 054022 (2000).
[58] M. Hentschinski, K. Kutak, and A. van Hameren, Forward Higgs production within high energy factorization in the heavy quark limit at next-to-leading order accuracy, Eur. Phys. J. C **81**, 112 (2021).
[59] M. Hentschinski, J. D. Madrigal Martínez, B. Murdaca, and A. Sabio Vera, The next-to-leading order vertex for a forward jet plus a rapidity gap at high energies, Phys. Lett. B **735**, 168 (2014).
[60] G. Chachamis, M. Hentschinski, J. D. Madrigal Martinez, and A. Sabio Vera, Gluon Regge trajectory at two loops from Lipatov's high energy effective action, Nucl. Phys. **B876**, 453 (2013).
[61] M. Hentschinski and A. Sabio Vera, NLO jet vertex from Lipatov's QCD effective action, Phys. Rev. D **85**, 056006 (2012).